Remote Sensing of Environment 146 (2014) 36–48

Contents lists available at ScienceDirect

Remote Sensing of Environment

journal homepage: www.elsevier.com/locate/rse

Retrieval of the seawater reflectance for suspended solids monitoring in the East China Sea using MODIS, MERIS and GOCI satellite data

David Doxaran [a,*], Nicolas Lamquin [c], Young-Je Park [b], Constant Mazeran [c], Joo-Hyung Ryu [b], Menghua Wang [d], Antoine Poteau [a]

[a] Laboratoire d'Océanographie de Villefranche (LOV), CNRS/UPMC, 06230 Villefranche-sur-Mer, France
[b] Korea Ocean Satellite Center, KIOST, Ansan P.O. Box 29, Seoul 425-600, Republic of Korea
[c] ACRI-ST, 260 route du Pin Montard, 06904 Sophia Antipolis, France
[d] NOAA National Environmental Satellite, Data, and Information Service, Center for Satellite Applications and Research, College Park, MD 20740, USA

ARTICLE INFO

Article history:
Received 31 October 2012
Received in revised form 3 May 2013
Accepted 10 June 2013
Available online 8 October 2013

Keywords:
Ocean color remote sensing
Seawater reflectance
Profiling float
Coastal waters
Suspended sediment dynamics
East China Sea

ABSTRACT

The objectives of this study are to: (i) compare the potential of the Moderate Resolution Imaging Spectroradiometer (MODIS), the Medium Resolution Imaging Spectrometer (MERIS) and the Geostationary Ocean Color Imager (GOCI) in retrieving the particulate backscattering coefficient, robust proxy of the concentration of suspended particulate matter (SPM), in the turbid waters of the East China Sea, then (ii) combine ocean color satellite data to field data recorded by an autonomous bio-optical profiling float to reconstitute and explain the dynamics of SPM within the whole water column in the middle of the East China Sea. MODIS, MERIS and GOCI seawater reflectance products at green, red and near-infrared (NIR) wavelengths are generated using atmospheric correction algorithms designed for turbid coastal waters then compared. Good agreement is obtained in the green and red while significant differences are observed in the NIR. The standard GOCI algorithm and a new one based on a regional empirical relationship established using MODIS satellite data are both proved to perform well over the whole range of water turbidity. Finally the dynamics of SPM is reconstituted along a three-month period to highlight a steady-state and stratified situation before the overpass of a large typhoon which mixed the water column, destroyed the deep-chlorophyll maximum and enhanced resuspension of bottom sediments varying according to tidal cycles.

1. Introduction

The monitoring of fluxes and dynamics of suspended particles exported by rivers into the coastal ocean is required in order to track the transport and fate of pollutants and determine the impact on light availability within the water column, then on phytoplankton growth and primary production (e.g., Tang, Ni, Muller-Karger, & Liu, 1998). In terms of biogeochemical cycles, a crucial issue is to understand and quantify the potentially massive mineralization of the terrestrial organic carbon which may represent up to half the organic carbon buried in marine sediments at the global scale (Hedges, Keil, & Benner, 1997; Schlunz & Schneider, 2000). In practice, such a monitoring is difficult in highly dynamic and often remote coastal regions (e.g., tropical and Arctic estuaries and deltas) using field data, resulting in high uncertainties and unknowns concerning the fluxes and fate of terrestrial organic carbon (Schlunz & Schneider, 2000). Ocean color remote sensing represents an efficient way to complement scarce field measurements and monitor the transport of key biogeochemical substances such as suspended sediments, chlorophyll-a (Chla) and colored dissolved organic matter (CDOM) in river plumes (e.g., Del Castillo & Miller, 2008; Hu, Montgomery, Schmitt, & Muller-Karger, 2004).

Over the last decade, the capabilities of ocean color satellite sensors have improved and provide: (i) a spectral resolution covering at least the visible and near-infrared (NIR) spectral regions; (ii) a spatial resolution of several hundred meters adapted to the dimensions of large estuaries, river plumes and bays; and (iii) a temporal resolution from about one day for polar-orbit sensors to less than 1 h for geostationary sensors (Neukermans, Ruddick, & Greenwood, 2012, Neukermans et al., 2009) now allowing to partly filter the cloud cover and study processes related to daily tidal cycles. The most recent ocean color satellite sensors used in oceanographic studies are the Moderate Resolution Imaging Spectroradiometer (MODIS) with two sensors operational since 1999 (Terra) and 2002 (Aqua), and the MEdium Resolution Imaging Spectrometer (MERIS) which provided data from March 2002 to April 2012. The Geostationary Ocean Color Imager (GOCI) is the first geostationary ocean color satellite sensor. It is operational since April 2011 and probably combines the best specifications to study coastal waters with spatial and temporal resolutions of respectively 500 m and 1 h despite its limited number of spectral bands (8 with only two in the NIR region). Taking into account the respective technical specifications of each ocean color satellite sensor, algorithms have been

* Corresponding author. Tel.: +33 4 93 76 37 24; fax: +33 4 93 76 37 39.
E-mail address: doxaran@obs-vlfr.fr (D. Doxaran).

0034-4257/$ – see front matter © 2013 Elsevier Inc. All rights reserved.
http://dx.doi.org/10.1016/j.rse.2013.06.020

developed to (i) retrieve the multi-spectral seawater reflectance signal (Rrs, in sr^{-1}, for remote sensing reflectance, or normalized water-leaving radiance, nL_w in $mW \cdot cm^{-2} \cdot \mu m^{-1} \cdot sr^{-1}$) by applying the so-called atmospheric corrections of satellite data then (ii) estimate the concentration of suspended particulate matter (SPM) and other ocean biological and biogeochemical properties by inversion of the seawater reflectance signal. Over turbid coastal waters, these two processing steps are quite challenging. First the seawater reflectance signal is significant in both the visible and NIR spectral regions, by opposition to open ocean waters which can be used as black targets in the NIR bands for atmospheric correction purposes (Gordon & Wang, 1994; IOCCG, 2010). Second, there is no general relationship for the inversion of the Rrs signal into SPM concentration (e.g., Doxaran, Cherukuru, & Lavender, 2006, Doxaran, Froidefond, & Castaing, 2003) due to the natural spatio-temporal variations of SPM composition and size, thus inherent optical properties (Babin, Morel, Fournier-Sicre, Fell, & Stramski, 2003; Babin et al., 2003; Neukermans, Loisel, Mériaux, Astoreca, & McKee, 2012). As the Rrs signal tends to saturate with increasing SPM concentration at short and then at long wavelengths (Doxaran, Froidefond, Lavender, & Castaing, 2002; Shen et al., 2010; Shi & Wang, 2009), green, red then NIR spectral bands must be used, successively, to invert the Rrs signal into SPM concentration in low, moderately and highly turbid coastal waters, respectively (Doxaran et al., 2006; Nechad, Ruddick, & Park, 2010; Zhang, Tang, Dong, Song, & Ding, 2010). It means that wavelengths shorter than 500 nm are not necessarily needed to remotely sense SPM concentrations in such environments.

The present study is focused on moderately to highly turbid sediment-dominated waters which develop at the land–sea interface: river mouths, river plumes and estuarine environments where maximum turbidity zones usually form. The main objective is to determine whether the Rrs signal and then SPM concentration can be consistently retrieved from MODIS, MERIS and GOCI satellite data in such waters where SPM concentrations typically vary from 1 g m^{-3} to more than 1000 g m^{-3}. The two specific questions addressed are: (i) can we accurately correct for atmospheric and ocean surface effects on ocean color satellite data recorded at 550, 650 and 850 nm (spectral bands required to retrieve SPM from Rrs)? (ii) What are the potential and limits associated to operational ocean color SPM algorithms? This second question mainly concerns GOCI satellite data for which atmospheric correction and SPM retrieval algorithms have been only recently developed and implemented.

As a first step, existing atmospheric correction algorithms are applied to a selection of concomitant MODIS, MERIS and GOCI satellite data recorded during mainly cloud-free days in 2011 and 2012. The Rayleigh-corrected reflectance, i.e., satellite data not yet corrected for the aerosol contribution, which usually represents the most difficult part in the atmospheric corrections, and Rrs signals obtained at 550, 650 and 850 nm (green, red, and NIR) are compared in order to assess the performance of the applied atmospheric corrections and consistency between the different sensors.

As a second step, the considered satellite-derived Rrs products are related to field measurements (match-ups) of the particulate backscattering coefficient, b_{bp} in m^{-1}, used here as a robust proxy of the SPM concentration (Neukermans, Loisel, et al., 2012), within surface waters. The resulting relationships obtained between Rrs and b_{bp} allow one to assess the potential and limits of each sensor and corresponding atmospheric correction algorithm tested. Field measurements are provided by an autonomous bio-optical profiling float used to maximize the number of match-ups with satellite data and document the dynamics of water masses and SPM within the whole water column. As ocean color satellite observations are only representative of the near-surface layer in turbid waters (e.g., Ouillon, 2003), we finally discuss the potential and limits of ocean color satellite data to study the transport and dynamics of SPM in coastal waters directly influenced by river plumes.

2. Data and methods

2.1. Study area

The selected study area (Fig. 1) is the East China Sea which separates the east coast of China from the south-west coast of Korea, i.e., the geographical zone delimited by 29°N/120°E (south-west) and 36°N/128°E (north-east). This area is a wide and shallow continental shelf directly influenced by the Yangtze River discharge. The Yangtze River is one of the major world rivers in terms of terrestrial suspended matter and organic carbon input into the ocean. Its freshwater outflow discharge follows seasonal variations typical of tropical rivers: high river flow from June to September (wet season) and low river flow from November to March (dry season) (e.g., Chen, Li, & Shen, 2001). Fully functional since July 2012, the Three Gorges Dam is intended to reduce the potential for flood events downstream. The turbid plume of the Yangtze River extends over hundreds of kilometers and can easily be detected on ocean color satellite data (Fig. 1) (Shi & Wang, 2010). The transport and fate of suspended sediments exported by the river into the continental shelf are affected by tidal currents (Shi, Wang, & Jiang, 2011) and a complex regional circulation which results in the formation of maximum turbidity zones associated with intense resuspension processes (Shi & Wang, 2010; Wang et al., 2007). The East China Sea is also affected by typhoons at the end of the summer period (August to September), which migrate in the north direction and generate strong winds.

The turbid coastal waters surrounding the mouth of the Yangtze River have often been used as reference test sites for ocean color remote sensing purposes (e.g., Beardsley, Limeburner, Yu, & Cannon, 1985; Shen, Verhoef, Zhou, Salama, & Liu, 2010; Tang et al., 1998), notably to design an atmospheric correction algorithm for highly-turbid sediment-dominated waters using the shortwave infrared (SWIR) spectral bands of MODIS (Wang, 2007; Wang & Shi, 2007; Wang, Shi, & Jiang, 2012). The reason is the extreme range of turbidity in this area, mainly resulting from SPM concentrations spanning from less than 1 to several thousands of g m^{-3} within surface waters (Zhang et al., 2010). Moreover, this region has been selected as it is viewed by the GOCI sensor.

2.2. Satellite data

A first ocean color satellite dataset is composed of concomitant MODIS-Aqua, MERIS and GOCI images recorded on a selection of cloud-free days in 2011 (Table 1). These images were selected based on visual inspection to avoid potential haze and sun glint contaminations. Here only GOCI data recorded around local noon (03:16 GMT) were considered for comparisons with MODIS and MERIS products, although GOCI acquisitions are made at each hour between 09:00 and 16:00 local time. Typically on each selected day, the time difference between GOCI and MERIS data acquisition was <1.5 h; it varied between 1 and 2.5 h between GOCI and MODIS-Aqua. A second satellite dataset was composed of concomitant MODIS-Aqua and GOCI (03:16 GMT) images recorded on a selection of cloud-free days from July to October 2012, i.e., during the deployment period of the bio-optical profiling float (Table 2). The remote-sensing reflectance above surface signal (Rrs in sr^{-1}) was considered: it is obtained after atmospheric correction of the top-of-atmosphere (TOA) signal normalized to the solar downwelling irradiance and corrected for bidirectional effects at sea surface (Gordon, 2005; Morel & Gentili, 1991, 1993, 1996; Wang, 2006).

Level 1A (L1A) MODIS-Aqua data (R2010.0 reprocessing) were downloaded from the oceancolor.gsfc.nasa.gov website then processed using the SeaDAS (Version 6.4) software (seadas.gsfc.nasa.gov) to generate location and Level 1B (L1B) files, then Rrs(555), Rrs(645) and Rrs(859) Level 2 (L2) products. These three spectral bands are associated to a higher (respectively 500, 250 and 250 m) spatial

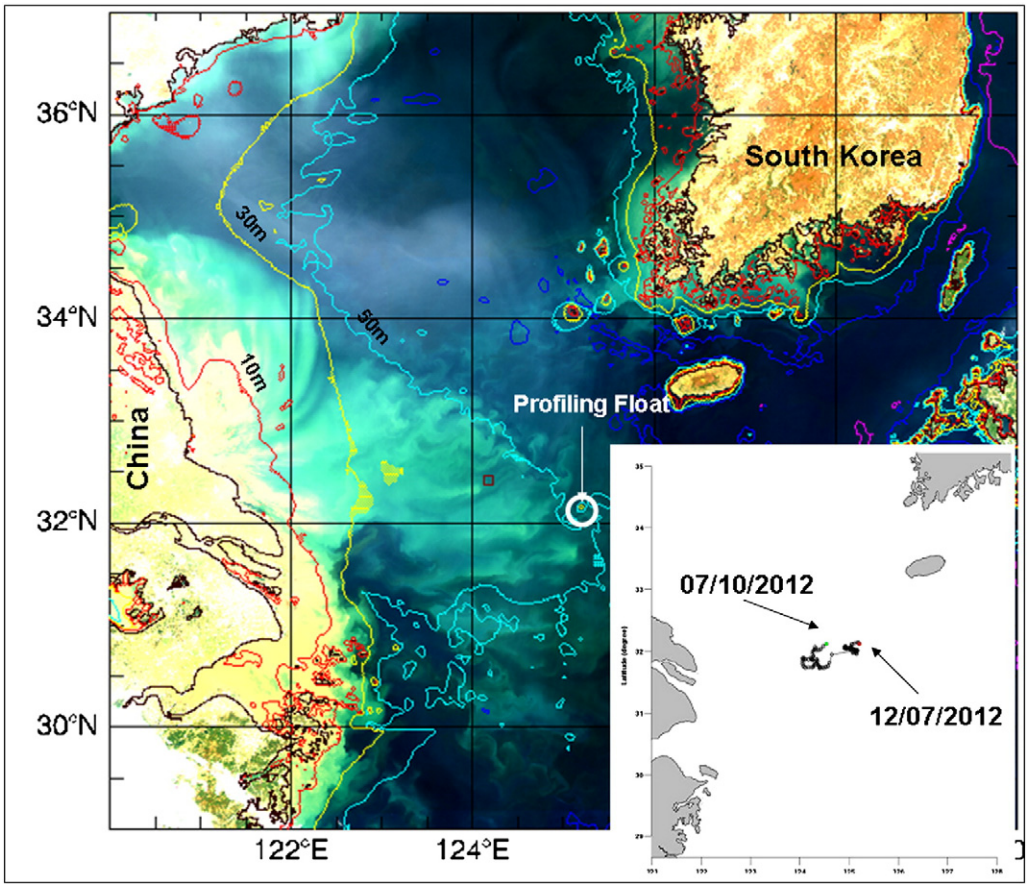

Fig. 1. RGB geo-referenced GOCI image of the study area and of the trajectory of the Provbio profiling float deployed on 11 July 2012.

resolution and have a lower sensitivity which avoids saturation problems in highly turbid sediment-dominated waters (e.g., Zhang et al., 2010). The NIR–SWIR atmospheric correction algorithm (Wang & Shi, 2007) was applied, as this algorithm is the most adapted in the case of highly scattering turbid waters. It uses the Rayleigh-corrected reflectance recorded at the SWIR bands (i.e. 1240 and 2130 nm, spatial resolution of 1 km averaged from 500 m) to determine the aerosol contribution assuming the water-leaving reflectance is negligible at these two wavelengths independently of water turbidity (Wang, 2007). Note that out of the three satellite sensors considered in the present study only MODIS has spectral bands in the SWIR. In order to avoid masking the most turbid waters, the default threshold values used to mask the sun glint and clouds were slightly (from 0.005 and 0.027 up to 0.02 and 0.1, respectively) in the case of images not affected by glint or clouds based on visual inspection.

Level 1 (L1) MERIS data from the 3rd reprocessing (Lerebourg & Bruniquel, 2011) were downloaded through the ODESA online facility

Table 1
Description of the 2011 ocean color satellite dataset. For each date, the GOCI data used are those recorded around noon (local time, i.e., 03:16 UT) and Δt (±hh:mm) is the time difference with MERIS and MODIS-Aqua satellite data acquisitions.

Day in 2011	GOCI (UT in hh:mm)	MERIS (Δt in hh:mm)	MODIS-Aqua (Δt in hh:mm)
5 April	03:16	–	+02:19
11 April	03:16	−00:40	+01:44
12 April	03:16	–	+02:24
4 September	03:16	−01:31	+01:29
6 September	03:16	−01:04	+01:29
7 September	03:16	−01:29	–
23 September	03:16	−01:25	+01:59
4 October	03:16	−01:27	+01:44
8 October	03:16	−00:33	+01:19
17 October	03:16	−01:02	+01:14
14 November	03:16	−01:26	+01:34
26 November	03:16	−01:28	+01:59

Table 2
Description of the 2012 Provbio and ocean color satellite datasets. For each date, the Provbio surfacing time (UT) is indicated and Δt (±hh:mm) is the time difference with GOCI and MODIS-Aqua satellite data acquisitions.

Day in 2012	Provbio (hh:mm UT)	GOCI (Δt in hh:mm)	MODIS-Aqua (Δt in hh:mm)
28 July	03:34	−00:28	+02:01
1 August	03:40	−00:24	+01:55
3 August	03:39	−00:23	–
6 August	03:16	00:00	+02:14
10 August	03:26	−00:10	+01:39
18 August	03:28	−00:12	+01:17
26 August	03:27	–	+01:38
31 August	03:22	−00:06	+02:03
1 September	03:19	−00:03	–
4 September	03:19	−00:03	–
10 September	03:20	–	+01:00
18 September	03:24	−00:08	–
19 September	03:24	−00:08	+01:49
20 September	03:27	−00:11	+01:33
23 September	03:25	−00:09	+01:55
24 September	03:20	−00:04	+01:15
25 September	03:18	−00:02	+01:57
30 September	03:18	–	–
1 October	03:20	–	+01:20
2 October	03:20	–	02:05
7 October	03:21	−00:05	+02:19

(earth.eo.esa.int/odesa) and processed to L2 with the ODESA software (Lerebourg & Bruniquel, 2011) including the 3rd reprocessing processor (MEGS.8) to get the normalized remote-sensing reflectance. The MERIS atmospheric correction is based on two sequential algorithms: first the Bright Pixel Atmospheric Correction (BPAC) (Moore & Lavender, 2011) which removes any residual marine signal in the NIR bands, then the Clear water Atmospheric Correction (Antoine & Morel, 1999) which determines the aerosol contents and type and yields to the normalized water-leaving reflectance at 560, 665 and 865 nm with a spatial resolution of 1.2 km.

GOCI L1B data and the GOCI Data Processing System (GDPS) software were provided by the Korea Ocean Satellite Center (KOSC) through the kosc.kordi.re.kr/index.kosc website. First, the standard (recently updated) KOSC algorithm (Ahn, Park, Ryu, Lee, & Oh, 2012) was used to produce normalized remote sensing reflectances at GOCI 555, 660 and 865 nm wavebands (spatial resolution of 500 m). A second atmospheric correction algorithm was applied to GOCI data to extend the comparisons with MODIS and MERIS products. This algorithm (Wang et al., 2012, 2013), not yet implemented into GDPS, has been developed based on a regional empirical relationship between the NIR normalized water-leaving radiance (nL_w) and diffuse attenuation coefficient at the wavelength of 490 nm ($K_d(490)$) derived from the long-term (2002–2009) MODIS-Aqua products generated using the SWIR atmospheric correction over the coastal waters in the GOCI covered western Pacific region. As described in Wang et al. (2012, 2013), the GOCI data processing uses the two NIR bands for atmospheric correction (Gordon & Wang, 1994), while the NIR water-leaving radiance contributions are estimated and removed using empirical relationships between (a) $nL_w(745)$ vs. $K_d(490)$ derived from NIR nL_w data using $K_d(490)$ from Wang, Son, and Harding (2009) method and (b) $nL_w(865)$ vs. $nL_w(745)$. This method was here applied to GOCI data recorded on two dates (11 April and 4 October 2011) to retrieve nL_w at wavelengths of 555, 660 and 865 nm and comparisons with the corresponding MERIS and MODIS nL_w products. It should be noted that the algorithm performance has the limitation (true for all data discussed here) for extremely turbid waters with $K_d(490) > \sim 5\ m^{-1}$, e.g., some cases over the Hangzhou Bay in the winter season. For such cases, normalized water-leaving radiance at the red band $nL_w(645)$ is saturated (Shen, Salama, et al., 2010; Shi & Wang, 2009), i.e., $nL_w(645)$ will not increase with increase of water turbidity. In fact, for such highly turbid waters, even the nL_w for the MODIS SWIR 1240 nm band is significant and not negligible (Shi & Wang, 2009).

As in Lamquin, Mazeran, Doxaran, Ryu, and Park (2012), no spectral correction was applied to correct for the slight band-shifts between MODIS, MERIS and GOCI. All satellite products were finally projected and averaged on the same regular grid with a step of 0.01° for a pixel-by-pixel comparison.

2.3. Field data

In order to maximize the number of match-ups between field and satellite data over a limited period of time, an autonomous bio-optical profiling float was deployed in the study area. This Provbio float (www.oao.obs-vlfr.fr/robots-a-sensorssm/profiling-floatssm/bio-sopticalpf) has been initially designed and used in the open ocean (Xing et al., 2011) but also proved to be operational, with some obvious limits, in coastal waters (Lorthiois, Doxaran, & Chami, 2012). To summarize, a Provbio is a free-drifting profiling float equipped with an iridium antenna for communication, a CTD sensor and a set of miniaturized bio-optical sensors to measure at a 1 m vertical resolution.

One Provbio was deployed on 11 July 2012 in the middle of the East China Sea (32.12°N/125.18°E) to profile three times a day at a speed of about 0.2 m s^{-1} and surface at 06:00, 12:00 and 18:00 local time. When not profiling, the float was programmed to ground at the bottom to minimize its drifting with currents. The float was equipped with the following sensors: one SBE 41 CTD probe (Seabird Inc.), one OCR-504 radiometer (Satlantic Inc.) to measure downwelling irradiance at three wavelengths (412, 490 and 555 nm), one ECO-FL2 sensor (Wetlabs Inc.) to measure fluorescence of CDOM and Chla, one ECO-BB (Wetlabs Inc.) to measure the particulate backscattering coefficient at 532 nm, $b_{bp}(532)$ in m^{-1}, and one C-Rover (Wetlabs Inc.) to measure the light attenuation coefficient at 660 nm. After deployment, the Provbio almost maintained its geographical position up to the 26 August 2012 when a big typhoon (diameter larger than 500 km) successively overpassed the East China Sea and then Yellow Sea within three days. The Provbio float consequently migrated 40 km west and restarted profiling on 29 August 2012. Until the 22 October 2012 the Provbio moved west and then east around a loop (Fig. 1). Tidal height, wind speed and direction measured at Ieodo station where the float was deployed (see Fig. 1) (source: www.khoa.go.kr) were available to analyze the recorded Provbio data.

During this deployment period, 16 match-ups were identified for both MODIS-Aqua and GOCI data (Table 2). The corresponding time differences between Provbio and satellite data was systematically less than twenty minutes for GOCI but typically varied between one and two hours for MODIS-Aqua (Table 2). The exact longitude and latitude recorded by the float when surfacing at 03:16 (GMT) were used to select the corresponding pixels on MODIS and GOCI satellite images; the surrounding 8 pixels were used to calculate the Rrs standard deviation assumed to be representative of the Rrs uncertainty (20% on average). The Rrs products retrieved on these pixels were then compared to the $b_{bp}(532)$ values measured at 0.5 m depth by the float; the $b_{bp}(532)$ value measured just below (1.5 m depth) was used to calculate the $b_{bp}(532)$ standard deviation assumed to be representative of the $b_{bp}(532)$ uncertainty (26% on average).

From 12 July 2012 to 22 October 2012, the Provbio float made a total of 316 casts. The daily-updated technical information and data can be viewed at: http://www.obs-vlfr.fr/OAO/provbio/YEL_SE_B27_MANIP01/YEL_SE_B27_MANIP01.html.

3. Results and discussion

3.1. Intercomparison between satellite products

On a specific date corresponding to high freshwater discharge from the Yangtze River (23 September 2011), the mapped MODIS-Aqua, MERIS and GOCI Rrs(555) products are compared in terms of spatial coverage and magnitude (Fig. 2). This date corresponds to high seawater reflectance values over the maximum turbid zones surrounding the Yangtze River mouth and extending offshore over a 100 km distance, representing wide variations by a factor of 10. MODIS, MERIS and GOCI satellite products allow retrieving a seawater reflectance signal up to the coast. Over the whole region of interest, the GOCI Rrs product compares well to the MODIS and MERIS products, both qualitatively (turbidity features) and quantitatively (magnitude of the seawater reflectance). Over the most turbid waters of the region, the satellite Rrs(555) products are consistent with very similar turbidity patterns and values. This first comparison tends to highlight the adapted GOCI, MODIS and MERIS sensitivities and validity of the atmospheric corrections applied in highly turbid waters, at least in the green spectral region (555 nm).

These first results show that in the case of the highly turbid sediment-dominated waters analyzed here, the NIR–SWIR (MODIS), BPAC (MERIS) and new standard KOSC (GOCI) atmospheric correction methods allow retrieving consistent Rrs values from MODIS and MERIS data recorded at 555 and 560 nm, respectively.

The recent Wang et al. (2012, 2013) atmospheric correction algorithm provides interesting results as it allows retrieving GOCI nL_w products over the whole range of water turbidity encountered in the East China Sea (Fig. 3). Moreover, first comparisons (here on images recorded on 11 April 2011) show the consistency of these new GOCI products with MODIS-Aqua nL_w products at green and red wavebands.

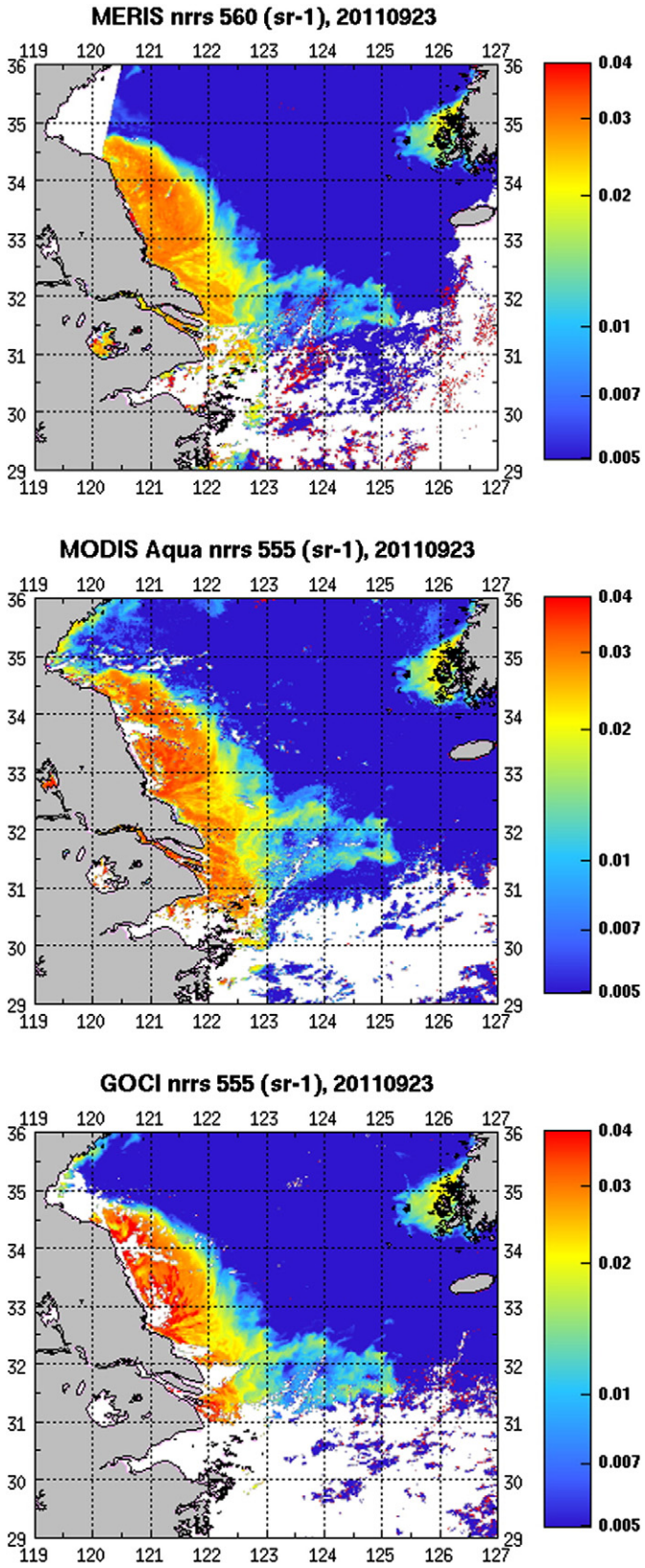

Fig. 2. MERIS, MODIS-Aqua and GOCI normalized remote-sensing reflectance products (Rrs(560), in sr^{-1}) on 23 September 2011.

This consistency is obvious in moderately to highly turbid waters and at visible wavebands, while significant differences can be observed over the less turbid waters of the region and in the NIR.

The next logical step is to qualitatively compare the Rrs products generated from MERIS and GOCI to the corresponding MODIS-Aqua Rrs products used here as reference. These comparisons are first made considering the selected cloud-free days in 2011 (Table 1). The MERIS and GOCI Rrs (560, 665 and 865 nm) products are successively compared based on density scatter-plots produced considering the whole study area (cf. Figs. 2 and 3), at selected dates then combining all the dates (Figs. 4 and 5, respectively). The acquisition time differences resulting in natural variations of water turbidity and atmospheric composition must be taken into account when comparing these satellite products.

Quite similar results are obtained when comparing the MERIS and MODIS-Aqua Rrs (555, 645 and 850 nm) products (Fig. 4 and Table 3). The agreement is good in visible spectral bands with some dispersion but slopes of the established linear relationship close to 1 with no significant biases observed. Once again the main differences are observed in the NIR where the MERIS Rrs(865) product systematically overestimates the corresponding MODIS Rrs(859) product by up to 80%. At this point it is difficult to conclude regarding which NIR seawater reflectance signal is over- or underestimated. However, it should be noted that the MERIS Rrs(865) is estimated using the model which may have limitation over such highly turbid waters, while the SWIR-based approach derives the NIR Rrs directly from MODIS measurements.

Satisfactory results are obtained when comparing GOCI to MODIS-Aqua Rrs (555, 645 and 850 nm) products (Fig. 5 and Table 3). The slopes of the obtained linear relationships are close to 1 at 555 nm and 645 nm but lower than 0.2 in the NIR (i.e., GOCI Rrs(865) is on average 80% lower than MODIS Rrs(859). In order to explain such unexpected differences in the NIR, comparisons were then made only considering the most turbid waters of the region, i.e., at the mouth of the Yangtze River and surrounding maximum turbidity zones (not shown). Rayleigh-corrected reflectances and Rrs satellite products at 860 nm were compared. Only images unaffected by suspicious contaminations (e.g., residual sun glint, haze, borders of clouds) were used. The results obtained were then much better and more convincing and linear relationships were established ($R^2 > 0.9$, slopes close to 1 and negligible intercept) between the GOCI, MODIS and MERIS Rrs products in the NIR. Therefore the use of such long NIR wavebands (860 nm) is limited to highly turbid waters. The low seawater signal retrieved in moderately turbid to clear waters (offshore) is significantly affected by residual errors in the atmospheric corrections, due to imperfect removal of the aerosol contribution.

Now considering the Wang et al. (2012) algorithm applied to GOCI data, the results obtained are also conclusive (Fig. 6). The slopes of the linear relationships established at visible wavelengths (555 and 645 nm) are both close to 1 (within a few percents) on the two selected dates (11 April and 4 October 2011). Note that a slight sun glint contamination was suspected on the 11 April 2011 MODIS-Aqua image, over the most turbid waters along the Chinese coast, but assumed to be negligible. Once again the results are not really conclusive in the NIR where differences as high as 70% are observed on both dates (see explanations in previous paragraph).

To summarize, based on a comparison between ocean color satellite seawater reflectance products, the potential of MODIS-Aqua and MERIS and associated NIR–SWIR and BPAC atmospheric corrections algorithms to retrieve consistent results in the moderately to highly turbid waters of the East China Sea has been demonstrated, at least at the green and red wavelengths. In the NIR, the rather low seawater signal and differences between satellite data acquisition times prevent from assessing the consistency of the seawater satellite products. The use of the NIR seawater reflectance signal is therefore limited to highly turbid waters. Based on comparisons with MODIS and MERIS products, the consistency and sensitivity of GOCI Rrs products produced using the new KOSC atmospheric correction algorithm (Ahn et al., 2012) have been highlighted over the moderately to highly turbid waters of the East China Sea. The new algorithm developed by Wang et al. (2012, 2013)

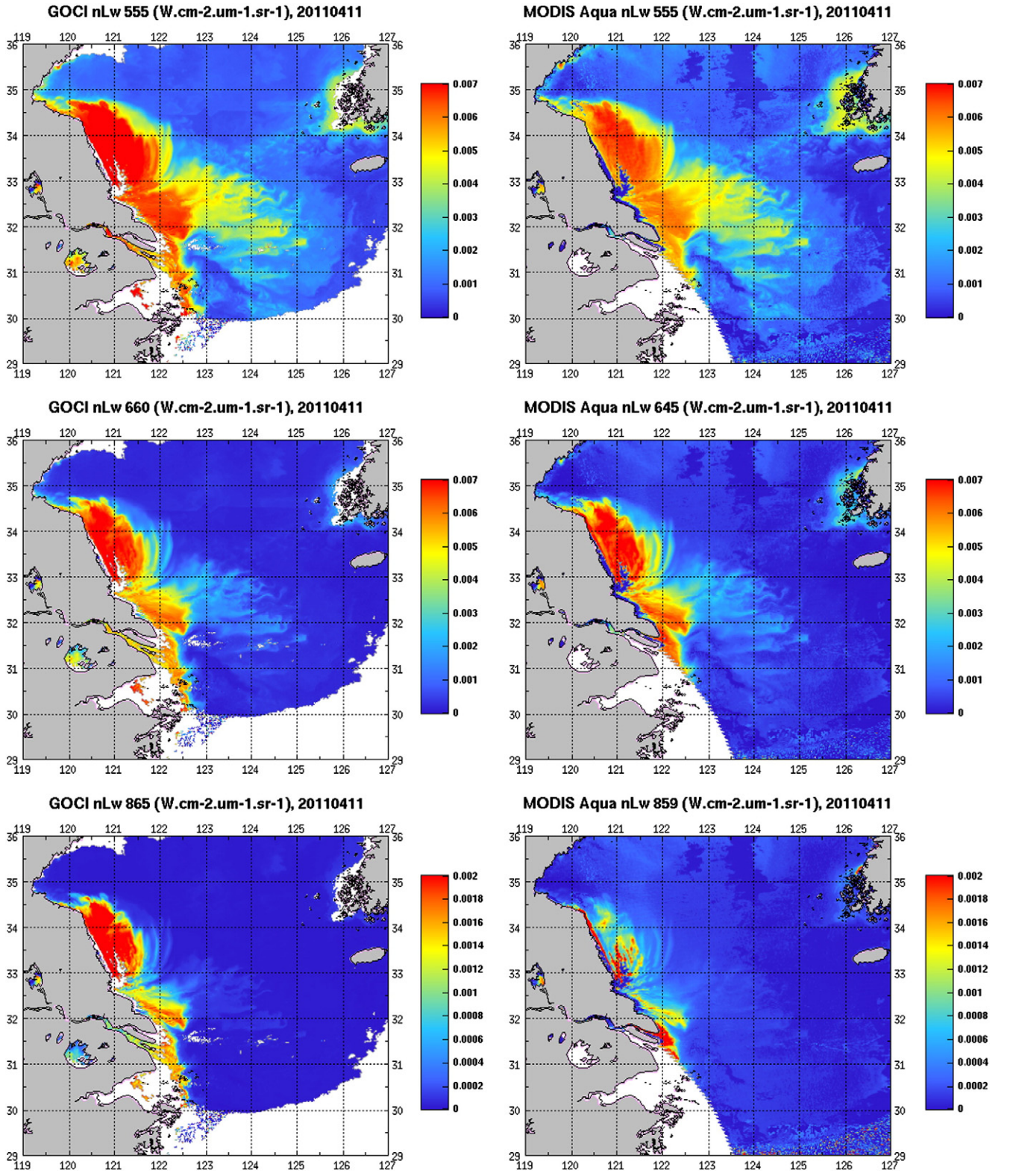

Fig. 3. GOCI normalized water-leaving radiance products (nL_w, in mW cm^{-2} μm^{-1} sr^{-1}) from Wang et al. (2012, 2013) atmospheric correction algorithm (GOCI-W) (left). The corresponding MODIS-Aqua nL_w products (right) have been processed using the NOAA-MSL12 ocean color data processing system. The date is 11 April 2011.

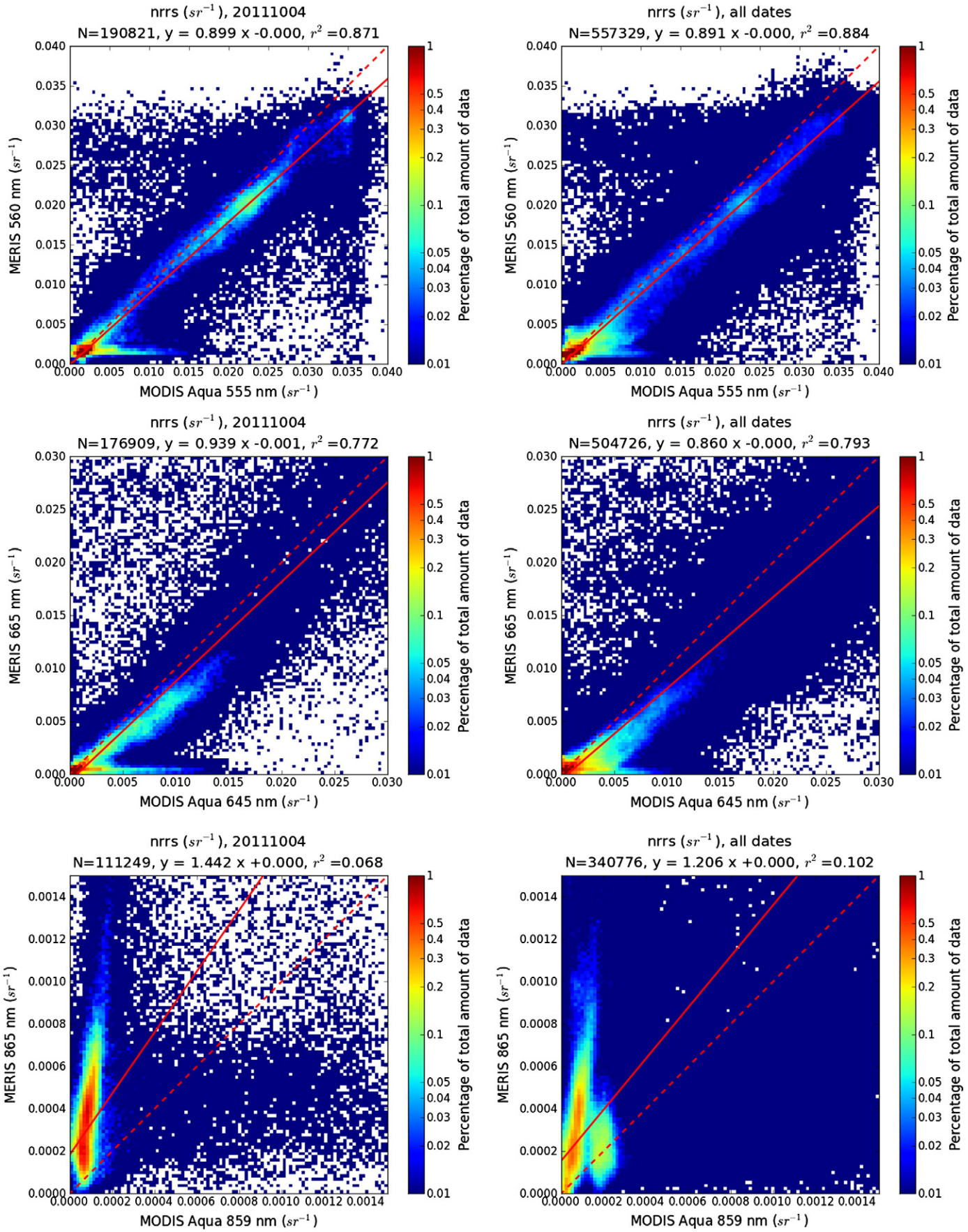

Fig. 4. Plots of Rrs(560), Rrs(665) and Rrs(865) from MERIS vs. Rrs(555), Rrs(645) and Rrs(859) from MODIS-Aqua (from top to bottom) on: 4 October 2011 (left) and for the combined three following dates: 23 September, 4 October and 17 October 2011 (right).

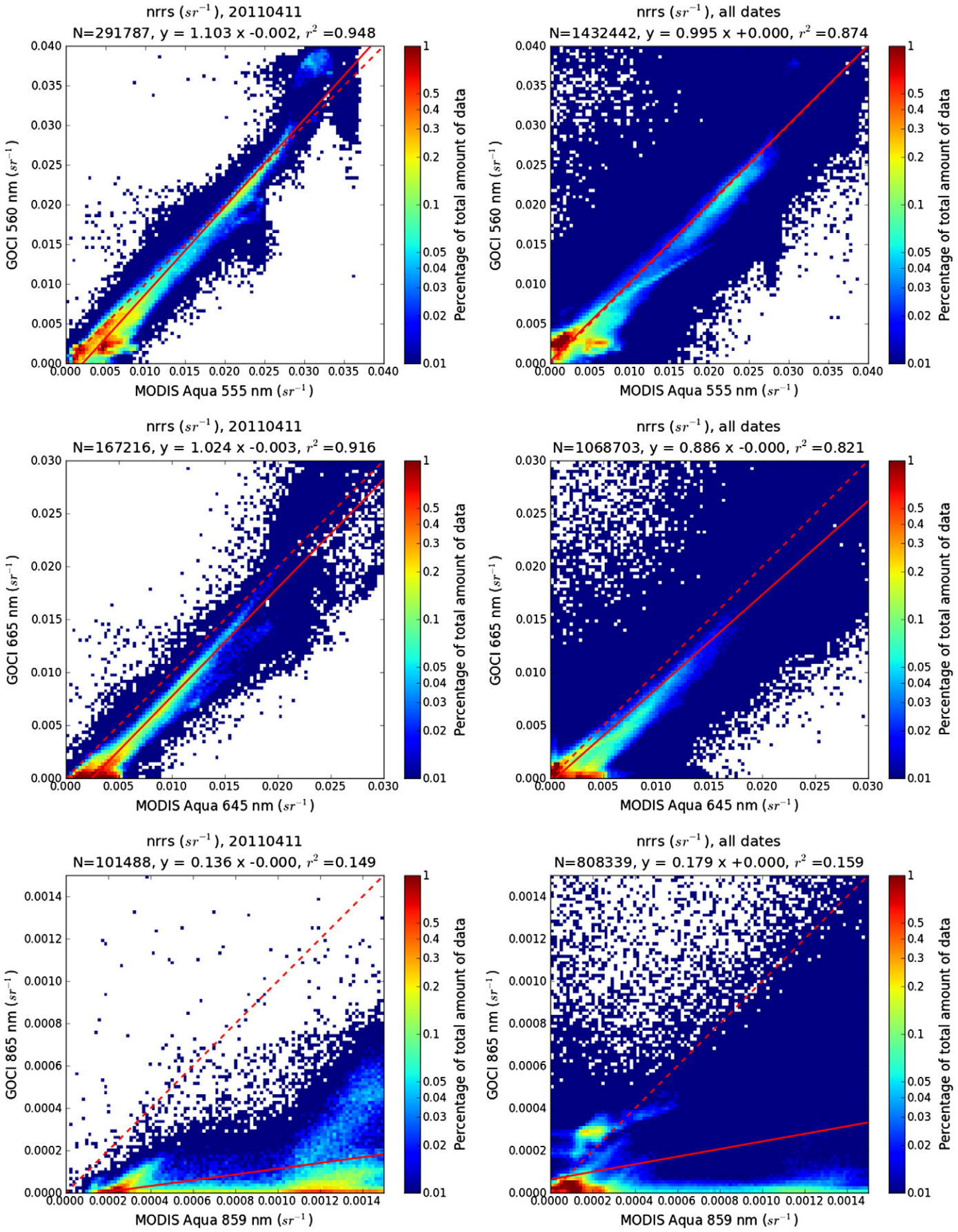

Fig. 5. Plots of Rrs(555), Rrs(660) and Rrs(865) from GOCI (new standard KOSC atmospheric correction) vs. Rrs(555), Rrs(645) and Rrs(859) from MODIS-Aqua (from top to bottom) on: 11 April 2011 (left) and for all dates listed on Table 1 (right).

Table 3
Slopes, intercepts and determination coefficients of regression analyses (linear relationships) obtained between the considered MERIS, GOCI and GOCI-W (y-axis) and corresponding MODIS-Aqua (x-axis) Rrs products. MERIS data were corrected for atmospheric effects by the combined bright pixel and clear water atmospheric correction (Antoine & Morel, 1999; Moore & Lavender, 2011), MODIS-Aqua by the NIR–SWIR (Wang & Shi, 2007) method and GOCI data by the new KOSC standard (Ahn et al., 2012) algorithm (GOCI) and the Wang et al. (2012, 2013) algorithm (GOCI-W). Regression analyses combine all dates listed in Table 1 and each regression was established for at least 650000 pixel-to-pixel comparisons.

Rrs (sr^{-1})	MODIS-Aqua 555 nm	MODIS-Aqua 645 nm	MODIS-Aqua 859 nm
MERIS	0.89/0.00/0.88	0.86/0.00/0.79	1.21/0.00/0.10
GOCI	0.99/0.00/0.87	0.89/0.00/0.82	1.08/0.00/0.89
GOCI-W	1.12/0.00/0.90	0.18/0.00/0.16	1.74/0/0.61

also provides satisfactory results and demonstrates the potential of GOCI data to detect turbidity variations over the whole range encountered in the highly turbid waters of the Yangtze River plume.

3.2. Assessment of satellite seawater reflectance products based on match-ups with field data

The next step to assess the performance of MODIS, MERIS and GOCI ocean color satellite products is to compare the satellite-derived Rrs to ground-truth, i.e., to coincident field optical measurements. While high quality seawater reflectance measurements were not available over the study area, match-ups with particulate light backscattering (b_{bp}) measured onboard the Provbio profiling float can be related to the ocean color satellite seawater reflectance products. The available $b_{bp}(532)$ field measurements provide a robust proxy of the SPM concentration (e.g., Neukermans, Loisel, et al., 2012). In moderately to highly turbid coastal waters, the Rrs signal is expected to present a linear relationship with SPM concentration while Rrs tends to saturate at high SPM concentration at short visible wavebands (at about 10 and 50 g m^{-3} at 555 and 645 nm, respectively) but not in the NIR (Doxaran et al., 2002; Nechad et al., 2010; Shen, Salama, et al., 2010). Here we rely on match-ups established in 2012 between satellite (only MODIS-Aqua and GOCI, as MERIS is no longer operational) and field (Provbio) data (Table 2).

A linear relationship can be established between the Rrs(555) signal retrieved from MODIS-Aqua and $b_{bp}(532)$ measured by the Provbio (Fig. 7). However the associated determination coefficient (R^2) is not satisfactory (0.62). This is mainly due to two series of match-up points significantly below and above, respectively, the mean linear relationship and corresponding to $b_{bp}(532)$ values in the range 0.05–0.09 m^{-1}, i.e., to moderately turbid waters. The time difference between the MODIS-Aqua and Provbio data acquisitions (up to 2 h) certainly explains most of the dispersion in the relationship established: within 2 h tidal currents can indeed significantly impact surface water turbidity (Wang et al., 2013). Also the signal measured onboard the float is not fully representative of the pixels sensed from satellites. At 645 nm, another linear relationship is established with a higher correlation ($R^2 = 0.76$, $N = 16$) which points out that the use of Rrs at red wavebands is usually appropriate to retrieve SPM concentrations in moderately turbid waters (Nechad et al., 2010). A significant correlation ($R^2 = 0.71$, $N = 16$) is still observed in the NIR despite the low Rrs(859) values retrieved from MODIS-Aqua data. In such moderately turbid waters low signal at SWIR wavelengths results in rather noisy Rrs(859) values and a NIR atmospheric correction (e.g., Bailey, Franz, & Werdell, 2010) may be more reliable. The NIR–SWIR atmospheric correction and retrieval of SPM concentration from the inversion of the Rrs(859) signal should be preferably considered in the case of highly turbid and reflective sediment-dominated waters (Doxaran, Froidefond, Castaing, & Babin, 2009, Doxaran et al., 2003) not yet sampled by the Provbio float.

Results could be expected to be better when considering match-ups established between the GOCI Rrs (generated using the standard KOSC algorithm (Ahn et al., 2012)) and Provbio $b_{bp}(532)$ data, as the satellite and field data were measured within a few minutes time difference (Table 2). It is actually the case at visible wavebands (Fig. 8) where linear relationships very similar to those established using MODIS-Aqua data are obtained with significantly less dispersion (R^2 of 0.85 and 0.93, at 560 and 665 nm, respectively). This result is quite encouraging as it once again demonstrates the consistency between MODIS-Aqua and GOCI Rrs products and the high potential of these products for the retrieval of SPM concentration in the moderately turbid waters of the East China Sea. Results obtained in the NIR are less satisfactory for GOCI than for MODIS-Aqua (R^2 of 0.65 instead of 0.71); moreover the slope of the linear relationship established between Rrs(865) and $b_{bp}(532)$ is half that obtained using Rrs(859) MODIS-Aqua data.

These first results obtained when comparing satellite-derived Rrs products to 'ground-truth', i.e., to field measurements of particulate backscattering within surface waters are encouraging and clearly demonstrate the potential of both MODIS and GOCI for the estimation of SPM concentrations and monitoring of SPM dynamics in the East China Sea.

3.3. Limits of ocean color satellite observations

It is now interesting to better understand the SPM dynamics in this area based on observations representative of the whole water column, then to determine what can be detected from space using ocean color remote sensing data and what will be missed by satellite observations limited to surface waters.

The salinity, $b_{bp}(532)$ and Chla fluorescence data measured by the Provbio float allow observing the dynamics of the water masses, SPM and phytoplankton, respectively, along the whole water column from 12 July 2012 to 22 October 2012 (Fig. 9). Note that the float was deployed in a shallow part (50 m water depth) of the East China Sea known as a maximum turbidity zone where SPM, notably those supplied by the Yangtze River, tend to accumulate and settle, while strong winds and currents contribute to the resuspension of bottom sediments.

From mid-July to end of August, the water mass was highly stratified, both in terms of density, salinity and SPM concentration, with low salinity waters within the surface layer while SPM, mainly suspended sediments, were concentrated within a bottom nepheloid layer (Fig. 9). A subsurface chlorophyll maximum (SCM) was clearly observed from 10 to 20 m water depth, with low Chla concentrations in the rest of the water column. This rather stable situation was maintained up to the overpass of the typhoon (26 to 28 August 2012) (see Section 2.3). The strong winds (wind speed up to 40 m s^{-1}, daily average on 27 August) associated with this typhoon significantly mixed the water column. As a result, the SCM almost instantaneously disappeared (see Wu, Platt, Tang, and Sathyendranath, 2007 for detailed explanation of such a phenomenon). Resuspension of bottom sediments occurred at the same time as spring tides so that SPM did propagate along the water column up to the surface. Then as the tidal range decreased suspended sediments started to settle. Also as a result of the typhoon overpass, the float moved 40 km westwards within three days, up to shallower waters (40 m depth) closer to the Yangtze River mouth. A change was then observed within the whole water column as salinity became almost constant from the surface to the bottom (mixing) and $b_{bp}(532)$, thus SPM concentration, significantly increased from bottom to surface waters. All along the deployment period of the float, the influence of tidal currents on SPM dynamics was clear, with resuspension of sediments during spring tides and settlement of SPM during neap tides. The signature of these phenomena is typical of fortnightly tidal cycles (14 day period).

Gordon and McCluney (1975) defined the optical depth from which originates 90% of the signal which can be detected from space as the depth where only remains 37% of the downwelling irradiance just

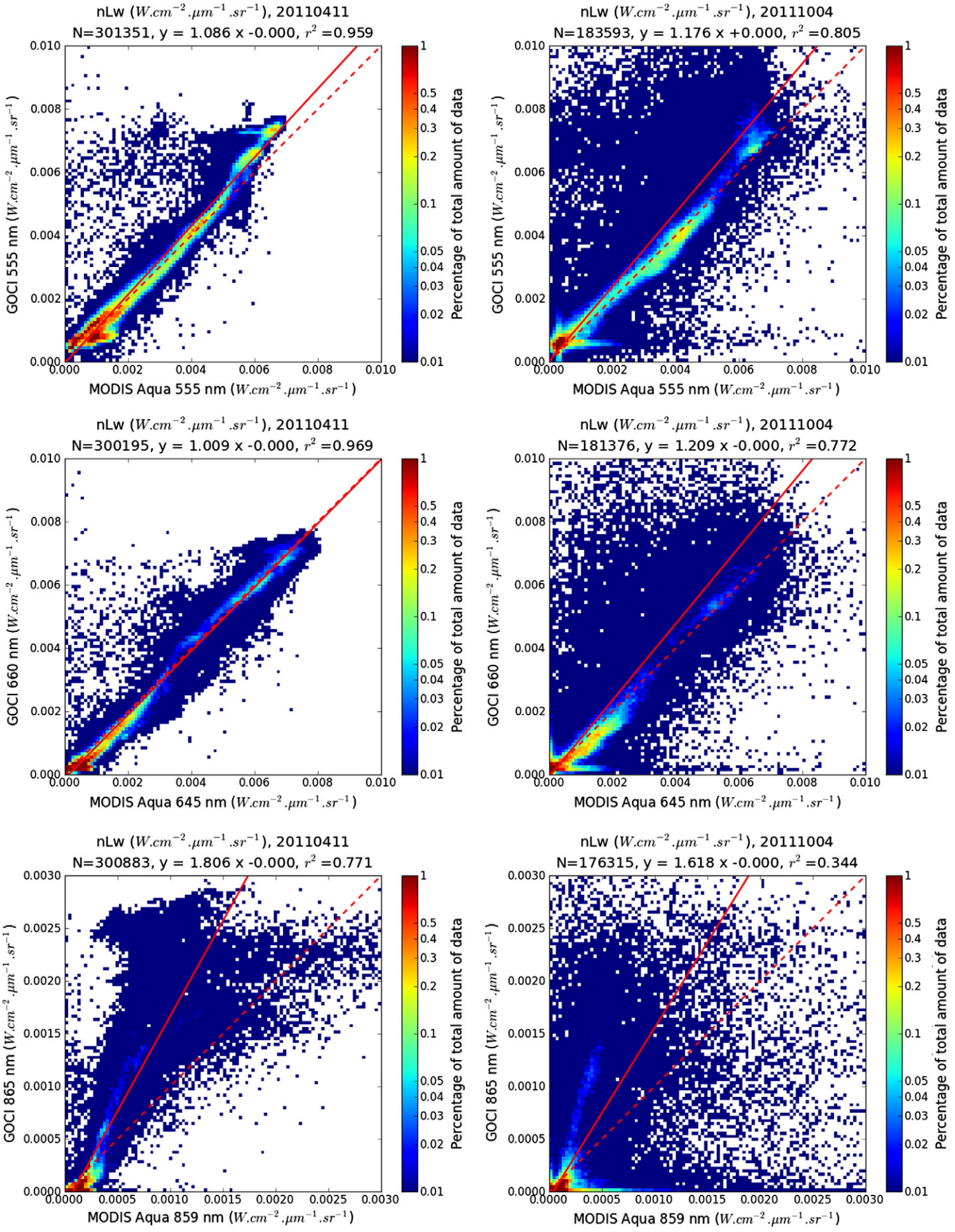

Fig. 6. Plots of Rrs(555), Rrs(660) and Rrs(865) from GOCI (Wang et al. (2012) atmospheric correction) vs. Rrs(555), Rrs(645) and Rrs(859) from MODIS-Aqua (NIR–SWIR atmospheric correction): on 11 April 2011 (left) and 4 October 2011 (right).

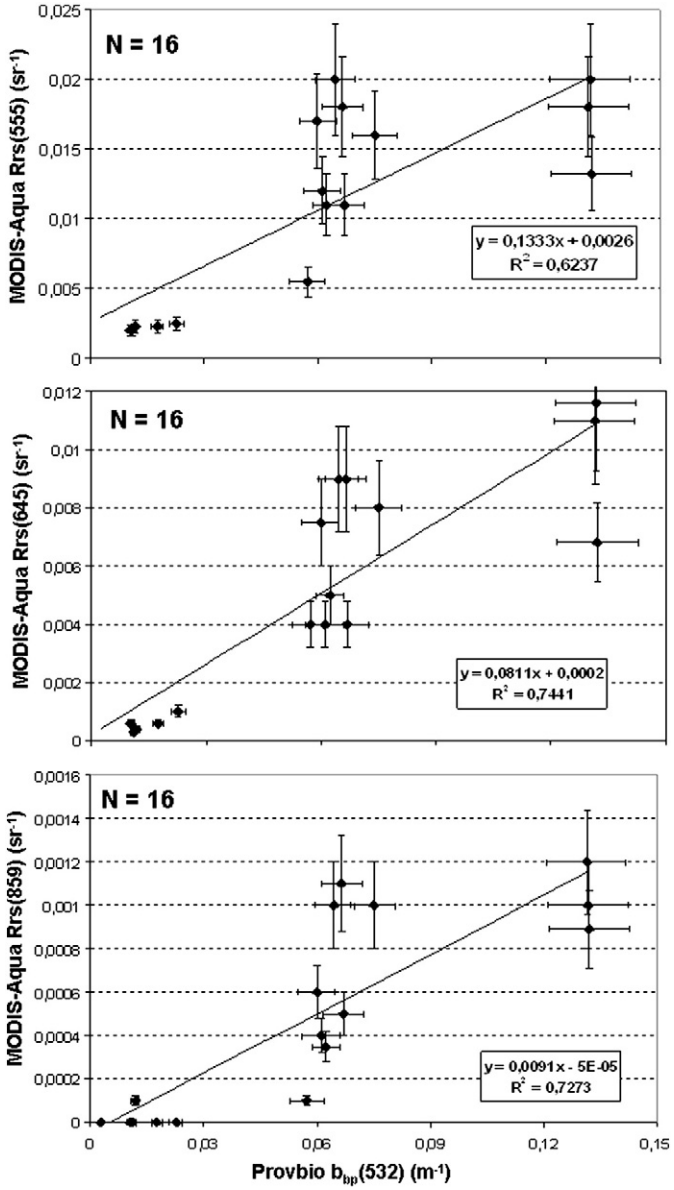

Fig. 7. Plot of MODIS-Aqua Rrs(555) (a), Rrs(645) (b) and Rrs(859) (c) as a function of surface (0–1 m depth) $b_{bp}(532)$ measured by the Provbio float (see Table 2 for match-ups details).

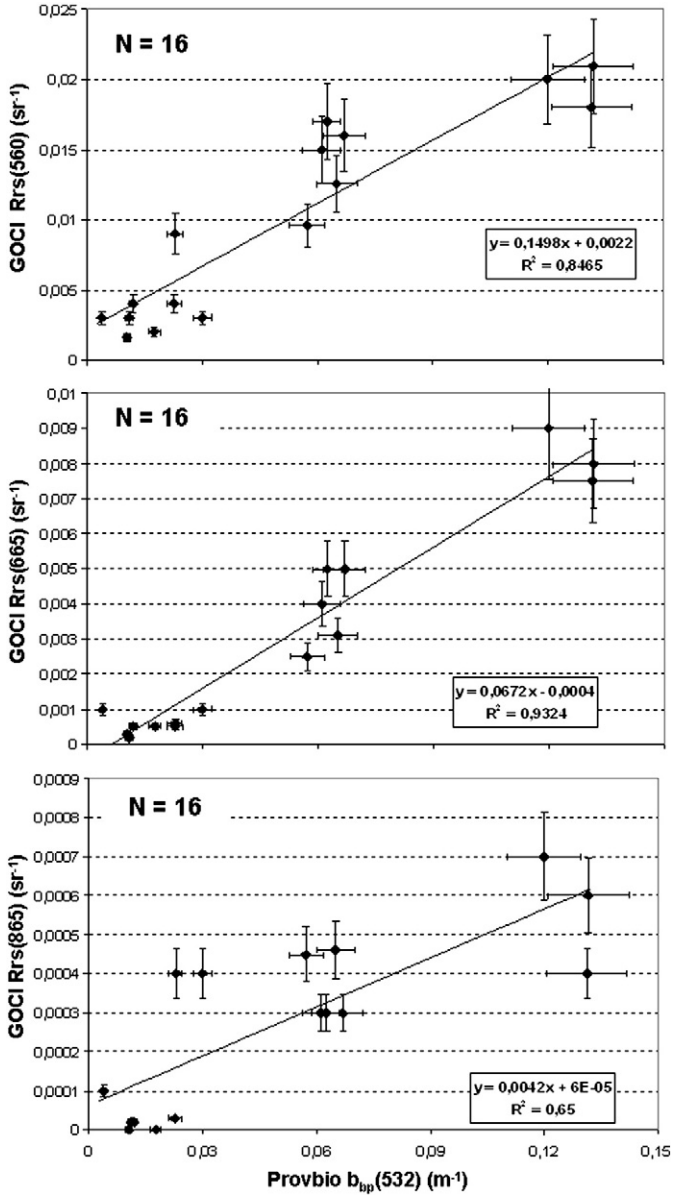

Fig. 8. Plot of GOCI Rrs(555) (a), Rrs(660) (b) and Rrs(865) (c) as a function of surface (0–1 m depth) $b_{bp}(532)$ measured by the Provbio float (see Table 2 for match-ups details).

below the surface. Based on downwelling irradiance measurements recorded onboard the Provbio (not shown), this optical depth at 555 nm was about 10 m before the typhoon event and reduced to about 5 m after the typhoon. This means that ocean color satellite data could not detect the SCM and resuspension processes before the typhoon. By comparison, after the storm, MODIS-Aqua and GOCI data could and have clearly detected the increase of SPM concentration within surface waters (Rrs(645) and Rrs(660) values higher than 0.005 sr^{-1} on Figs. 7 and 8) and its variations mainly related to the fortnightly tidal cycles. This highlights the potential and limits of ocean color satellite observations in turbid coastal waters, but also how complementary can be ocean color satellite and bio-optical autonomous profiling floats observations.

4. Conclusions

The objective of the study was to assess the consistency and capabilities of MODIS, MERIS and GOCI seawater reflectance products (at green, red and NIR wavebands) in the turbid waters of the East China Sea in order to estimate SPM concentrations and then monitor the dynamics of SPM in this complex coastal environment. The NIR–SWIR (Wang & Shi, 2007), BPAC (Moore & Lavender, 2011), new standard KOSC (Ahn et al., 2012), and Wang et al. (2012, 2013) atmospheric correction algorithms were applied, respectively, to MODIS, MERIS and GOCI satellite data recorded in 2011 and 2012 to retrieve the water-leaving signal.

Overall, a good consistency was observed between these different satellite products at visible wavelengths but significant differences were detected in the NIR. MODIS, MERIS and GOCI data products proved their consistency over the wide range of water turbidity encountered in the East China Sea, including over the most turbid waters surrounding the Yangtze River mouth. The capabilities of GOCI have been highlighted. First results presented in this study suggest that both the new KOSC standard (Ahn et al., 2012) and new algorithm designed by Wang et al. (2012, 2013) already represent a valuable solution in terms of atmospheric correction of GOCI data recorded over highly turbid waters.

The satellite-derived remote sensing reflectance products were then related to field measurements of the particulate backscattering coefficient (match-ups) within surface waters recorded onboard an

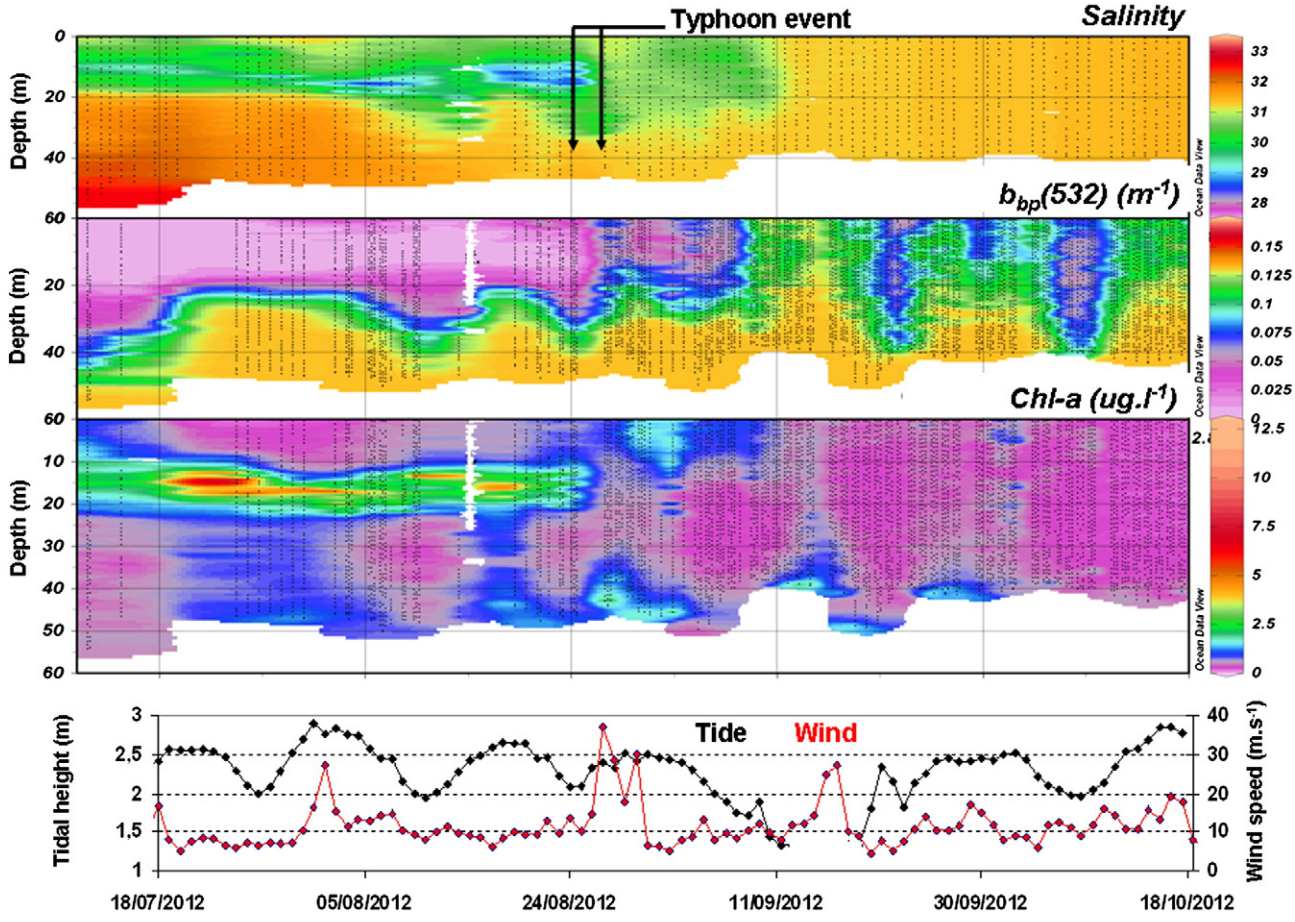

Fig. 9. Day-to-day variations of salinity, particulate backscattering ($b_{bp}(532)$, m^{-1}) and chlorophyll-a concentration (mg m^{-3} based on manufacturer calibration on phytoplankton culture, i.e., not in situ calibration) along the water column, in the middle of the East China Sea (see Fig. 1 for detailed location), measured by the Provbio profiling float from 12 July 2012 to 22 October 2012. Measurements have been interpolated using the Ocean Data View software (odv.awi.de). Daily averages of maximum tidal height (m) (no data from 11 to 20 September) and wind speed (m s^{-1}) were measured at leodo station where the float was deployed (see Fig. 1).
Source: www.khoa.go.kr.

autonomous bio-optical profiling float. Results proved that the use of a red wavelength (around 650 nm) is the most appropriate in order to accurately estimate the SPM concentration in the moderately turbid waters sampled ($b_{bp}(532) < 0.15$ m^{-1}), as already suggested by Nechad et al. (2010). Now an optimized SPM algorithm adapted to the wide variations of SPM concentrations would ideally be to switch from using Rrs at the green to red and even the NIR with increasing SPM concentration.

Our results suggest that MODIS, MERIS and GOCI satellite products, i.e., the normalized remote sensing reflectance signal in the red, can be combined and used to monitor the spatio-temporal dynamics of SPM in the East China Sea. Daily field measurements recorded along the water column over a three-month period in the middle of the East China Sea showed that vertical dynamics of water masses and suspended particles usually predominate over horizontal dynamics in this specific shallow (<50 m depth) area located 200 km away from the coasts. Also the potential of ocean color satellite observations, limited to about a 5 to 10 m thick surface layer, for the monitoring of SPM in the region has been demonstrated. In this study, ocean color satellite observations were combined with field measurements recorded by an autonomous bio-optical profiling float to obtain information from the whole water column. Such a float provides information on the stratification of water masses, resuspension of bottom sediments, deep-chlorophyll maximum and optical depth viewed by ocean color satellite sensors.

Future work will aim at developing a 'self-sufficient' atmospheric correction algorithm for GOCI data that would perform as well as the one developed by Wang et al. (2012, 2013) in highly turbid waters but would only rely on GOCI data. Another specific objective will be to better assess the quality of the NIR Rrs signal retrieved from MODIS, MERIS and GOCI data over highly turbid waters surrounding the Yangtze River plume. The next step will be to combine long-term ocean color satellite data with available field observations to monitor and better understand the SPM dynamics in the East China Sea over the last decade (2002–2012).

Acknowledgments

This study was funded by the Centre National d'Etudes Spatiales (CNES) through the GOYA, Provpanache and contract no. 116405 projects, EC FP7 AQUAMAR project, and represents a contribution to the PABO project (P.I. H. Claustre) funded by Agence Nationale de la Recherche.

References

Ahn, J. H., Park, Y. J., Ryu, J. H., Lee, B., & Oh, S. (2012). Development of atmospheric correction algorithm for Geostationary Ocean Color Image (GOCI). *Ocean Science Journal*, *47*(3), 247–259.

Antoine, D., & Morel, A. (1999). A multiple scattering algorithm for atmospheric correction of remotely-sensed ocean colour (MERIS instrument): Principle and implementation for atmospheres carrying various aerosols including absorbing ones. *International Journal of Remote Sensing*, *20*(9), 1875–1916.

Babin, M., Morel, A., Fournier-Sicre, V., Fell, F., & Stramski, D. (2003). Light scattering properties of marine particles in coastal and oceanic waters as related to the particle mass concentration. *Limnology and Oceanography*, *48*, 843–859.

Babin, M., Stramski, D., Ferrari, G. M., Claustre, H., Bricaud, A., Obolensky, G., et al. (2003). Variations in the light absorption coefficients of phytoplankton, non-algal particles, and dissolved organic matter in coastal waters around Europe. *Journal of Geophysical Research*. http://dx.doi.org/10.1029/2001JC000882.

Bailey, S. W., Franz, B.A., & Werdell, P. J. (2010). Estimation of near-infrared water-leaving reflectance for satellite ocean color data processing. *Optics Express*, *18*, 7521–7527.

Beardsley, R. C., Limeburner, R., Yu, H., & Cannon, G. A. (1985). Discharge of the Changjiang (Yangtze River) into the East China Sea. *Continental Shelf Research*, *4*, 57–76.

Chen, Z., Li, J., Shen, H., & Zhanghua, W. (2001). Yangtze River of China: Historical analysis of discharge variability and sediment flux. *Geomorphology*, *41*, 77–91.

Del Castillo, C. E., & Miller, R. L. (2008). On the use of ocean color remote sensing to measure the transport of dissolved organic carbon by the Mississippi River plume. *Remote Sensing of Environment*, *112*, 836–844.

Doxaran, D., Cherukuru, R. C. N., & Lavender, S. J. (2006). Inherent and apparent optical properties of turbid estuarine waters: Measurements, modelling and application to remote sensing. *Applied Optics*, *45*, 2310–2324.

Doxaran, D., Froidefond, J. M., & Castaing, P. (2003). Remote sensing reflectance of turbid sediment-dominated waters. Reduction of sediment type variations and changing illumination conditions effects using reflectance ratios. *Applied Optics*, *42*, 2623–2634.

Doxaran, D., Froidefond, J. M., Castaing, P., & Babin, M. (2009). Dynamics of the turbidity maximum zone in a macrotidal estuary (the Gironde, France): Observations from field and MODIS satellite data. *Estuarine, Coastal and Shelf Science*, *81*, 321–332.

Doxaran, D., Froidefond, J. M., Lavender, S. J., & Castaing, P. (2002). Spectral signature of highly turbid waters. Application with SPOT data to quantify suspended particulate matter concentrations. *Remote Sensing of Environment*, *81*, 149–161.

Gordon, H. R. (2005). Normalized water-leaving radiance: Revisiting the influence of surface roughness. *Applied Optics*, *44*, 241–248.

Gordon, H. R., & McCluney, W. R. (1975). Estimation of the sunlight penetration in the sea for remote sensing. *Applied Optics*, *14*, 413–416.

Gordon, H. R., & Wang, M. (1994). Retrieval of water-leaving radiance and aerosol optical thickness over the oceans with SeaWiFS: A preliminary algorithm. *Applied Optics*, *33*, 443–452.

Hedges, J. I., Keil, R. G., & Benner, R. (1997). What happens to terrestrial organic matter in the ocean? *Organic Geochemistry*, *27*, 195–212.

Hu, C., Montgomery, E. T., Schmitt, R. W., & Muller-Karger, F. E. (2004). The dispersal of the Amazon and Orinoco River water in the tropical Atlantic and Caribbean Sea: Observation from space and S-PALACE floats. *Deep-Sea Research II*, *51*, 1151–1171.

IOCCG (2010). Atmospheric correction for remotely-sensed ocean-colour products. In M. Wang (Ed.), *Reports of International Ocean-Color Coordinating Group, No.10*. Dartmouth, Canada: IOCCG.

Lamquin, N., Mazeran, C., Doxaran, D., Ryu, J. H., & Park, Y. J. (2012). Assessment of GOCI radiometric products using MERIS, MODIS and field Measurements. *Ocean Science Journal*, *47*(3), 287–311.

Lerebourg, C., & Bruniquel, V. (2011). MERIS 3rd data reprocessing software and ADF updates. *European Space Agency report, Ref A879.NT.008.* : ACRI-ST.

Lorthiois, T., Doxaran, D., & Chami, M. (2012). Daily and seasonal dynamics of suspended particles in the Rhône River plume based on remote sensing and field optical measurements. *Geo-Marine Letters*, *32*, 89–101. http://dx.doi.org/10.1007/s00367-012-0274-2.

Moore, G. F., & Lavender, S. J. (2011). Case IIS bright pixel atmospheric correction. MERIS ATBD 2.6, issue 5.0.

Morel, A., & Gentili, B. (1991). Diffuse reflectance of oceanic waters: Its dependence on Sun angle as influenced by the molecular scattering contribution. *Applied Optics*, *30*, 4427–4438.

Morel, A., & Gentili, B. (1993). Diffuse reflectance of oceanic waters II. Bidirectional aspects. *Applied Optics*, *32*, 6864–6879.

Morel, A., & Gentili, B. (1996). Diffuse reflectance of oceanic waters III. Implication of bidirectionality for the remote-sensing problem. *Applied Optics*, *35*, 4850–4862.

Nechad, B., Ruddick, K., & Park, Y. J. (2010). Calibration and validation of a generic multisensor algorithm for mapping of total suspended matter in turbid waters. *Remote Sensing of Environment*, *114*, 854–866.

Neukermans, G., Loisel, H., Mériaux, X., Astoreca, R., & McKee, D. (2012). In situ variability of mass-specific beam attenuation and backscattering of marine particles with respect to particle size, density, and composition. *Limnology and Oceanography*, *57*, 124–144. http://dx.doi.org/10.4319/lo.2011.57.1.0124.

Neukermans, G., Ruddick, K., Bernard, E., Ramon, D., Nechad, B., & Deschamps, P. -Y. (2009). Mapping total suspended matter from geostationary satellites: A feasibility study with SEVIRI in the Southern North Sea. *Optics Express*, *17*(16), 14029–14052.

Neukermans, G., Ruddick, K., & Greenwood, N. (2012). Diurnal variability of turbidity and light attenuation in the southern North Sea from the SEVIRI geostationary sensor. *Remote Sensing of Environment*, *124*, 564–580.

Ouillon, S. (2003). An inversion method for reflectance in stratified turbid waters. *International Journal of Remote Sensing*, *24*(3), 535–558.

Schlunz, B., & Schneider, R. R. (2000). Transport of terrestrial organic carbon to the oceans by rivers: Re-estimating flux and burial rates. *International Journal of earth Sciences*, *88*, 599–606.

Shen, F., Salama, S., Zhou, Y., Li, J., Su, Z., & Kuang, D. (2010). Remote-sensing reflectance characteristics of highly turbid estuarine waters? A comparative experiment of the Yangtze River and the Yellow River. *International Journal of Remote Sensing*, *31*(10), 2639–2654.

Shen, F., Verhoef, W., Zhou, Y., Salama, S., & Liu, X. (2010). Satellite estimates of wide-range suspended sediment concentrations in Changjiang (Yangtze) estuary using MERIS data. *Estuaries and Coasts*, *33*(6), 1420–1429.

Shi, W., & Wang, M. (2009). An assessment of the black ocean pixel assumption for MODIS SWIR bands. *Remote Sensing of Environment*, *113*, 1587–1597.

Shi, W., & Wang, M. (2010). Satellite observations of the seasonal sediment plume in central East China Sea. *Journal of Marine System*, *82*, 280–285.

Shi, W., Wang, M., & Jiang, L. (2011). Spring-neap tidal effects on satellite ocean color observations in the Bohai Sea, Yellow Sea, and East China Sea. *Journal of Geophysical Research*, *116*, C12932. http://dx.doi.org/10.1029/2011JC007234.

Tang, D. L., Ni, I. -H., Muller-Karger, F. E., & Liu, Z. J. (1998). Analysis of annual and spatial patterns of CZCS-derived pigment concentration on the continental shelf of China. *Continental Shelf Research*, *18*, 1493–1515.

Wang, M. (2006). Effects of ocean surface reflectance variation with solar elevation on normalized water-leaving radiance. *Applied Optics*, *45*, 4122–4128.

Wang, M. (2007). Remote sensing of the ocean contributions from ultraviolet to near-infrared using the shortwave infrared bands: Simulations. *Applied Optics*, *46*, 1535–1547.

Wang, M., Ahn, J. H., Jiang, L., Shi, W., Son, S., Park, Y. J., et al. (2013). Ocean color products from the Korean Geostationary Ocean Color Imager (GOCI). *Optics Express*, *21*, 3835–3849.

Wang, Z., Li, L., Chen, D., Xu, K., Wie, T., Gao, J., et al. (2007). Plume front and suspended sediment dispersal off the Yangtze (Changjiang) River mouth, China during non-flood season. *Estuarine, Coastal and Shelf Science*, *71*, 60–67.

Wang, M., & Shi, W. (2007). The NIR–SWIR combined atmospheric correction approach for MODIS ocean color data processing. *Optics Express*, *15*(24), 15722–15733.

Wang, M., Shi, W., & Jiang, L. (2012). Atmospheric correction using near-infrared bands for satellite ocean color data processing in the turbid western Pacific region. *Optics Express*, *20*(2), 741–753.

Wang, M., Son, S., & Harding, J. R. W., Jr. (2009). Retrieval of diffuse attenuation coefficient in the Chesapeake Bay and turbid ocean regions for satellite ocean color applications. *Journal of Geophysical Research*, *114*(C10). http://dx.doi.org/10.1029/2009JC005286 (C10011).

Wu, Y., Platt, T., Tang, C. C. L., & Sathyendranath, S. (2007). Short-term changes in chlorophyll distribution in response to a moving storm: A modelling study. *Marine Ecology Progress Series*, *335*, 57–68.

Xing, X., Morel, A., Claustre, H., Antoine, D., D'Ortenzio, F., Poteau, A., et al. (2011). Combined processing and mutual interpretation of radiometry and fluorimetry from autonomous profiling Bio-Argo floats. The retrieval of chlorophyll a. *Journal of Geophysical Research*, *116*. http://dx.doi.org/10.1029/2010JC006899 (C06020).

Zhang, M., Tang, J., Dong, Q., Song, Q. T., & Ding, J. (2010). Retrieval of total suspended matter concentration in the Yellow and East China Seas from MODIS imagery. *Remote Sensing of Environment*, *114*, 392–403.